

Timing jitter smoothing by Talbot effect.

II. Intensity spectrum

Carlos R. Fernández-Pousa and Felipe Mateos

División de Óptica, Departamento de Ciencia y Tecnología de Materiales, Universidad Miguel Hernández, Avenida Ferrocarril s/n, E03202 Elche (Alicante) Spain

Laura Chantada, María Teresa Flores-Arias, Carmen Bao, María Victoria Pérez,
and Carlos Gómez-Reino

Grupo de Óptica GRIN, Departamento de Física Aplicada, Universidade de Santiago de Compostela, Campus Sur, E15782 Santiago de Compostela, Spain

Received July 7, 2004; revised manuscript received November 3, 2004; accepted November 17, 2004

The power spectral density of the intensity of jittery trains after an integer temporal Talbot dispersive line is computed in the small-signal approximation. The influence in the spectrum of the optical linewidth and chirp of the Gaussian pulses of the train and also of different pulse-to-pulse timing jitter correlations is addressed. Before entering the Talbot dispersive line, timing jitter produces noise sidebands around the harmonics of the train. The temporal Talbot effect adds a multiplicative factor to the noise spectral density that depends on the characteristics of both the pulses and the dispersive line but not on the pulse-to-pulse correlation or the value of the timing jitter's standard deviation. The structure of this multiplicative term is peaked, resulting in narrowband noise patterns in specific locations of the spectrum and, in particular, around the harmonics of the train. Thus the temporal Talbot effect provides a dispersive mechanism for noise filtering. The bandwidth of the dispersion-induced noise peaks is ~ 1 order of magnitude below the repetition-rate frequency. © 2005 Optical Society of America

OCIS codes: 030.1670, 070.6760, 320.5550, 060.2340.

1. INTRODUCTION

The temporal Talbot effect is a well-established technique for the generation of high-repetition-rate trains of coherent pulses by use of a dispersive line.^{1–7} To be precise, multiplication of the repetition rate is obtained when a dispersive line creates a fractional Talbot replica of the original train. When the dispersive line is adjusted to create an integer Talbot replica, the Talbot dispersive line creates a replica of the original train and does not produce any increase in its repetition rate.

However, a Talbot replica of a train is a different picture of the original train. The replica is created by interference of the dispersed pulses of the initial train, so a specific pulse in the output train is formed by the interference of the neighboring pulses in the original train. This implies that the output train is a coherent average of the input, resulting in a self-restoration capability of the temporal Talbot effect when the dispersive line is fed with a nonideal train, which is a well-known fact in diffractive optics.^{8,9} Therefore the Talbot replicas of nonideal noisy trains can show intrinsic noise-smoothing features. Recently this self-restoration capability under timing jitter was explored.¹⁰ That examination was focused on the time domain, showing a smoothing of the jitter through flattening of the variance. Here we extend these results to the spectral domain.

Our objective in this paper is an analysis of the power spectral density of the intensity of integer Talbot-imaged trains when the original train suffers from tim-

ing jitter. This quantity is proportional to the radio-frequency (RF) noise measured in an electrical spectrum analyzer after direct detection of the train with an ideal receiver of infinite bandwidth. It is shown that specific portions of the initial noise content are filtered after the Talbot device. In particular, noise survives in the vicinity of the harmonics of the train, but, depending on the spectral bandwidth of the original noise spectrum, it can provide a dispersive mechanism for noise reduction. Noise is filtered up to offset frequencies that are ~ 1 order of magnitude below the frequency of the repetition rate. Additional narrowing of this bandwidth is obtained through an increase in either the integer Talbot index or the linewidth of the pulses. Thus the potential application of the effect is restricted to jittery trains with an initial broadband noise spectrum, high pulse linewidths, and highly dispersive lines.

These features have also been reported after an exact analysis of the spectral content of the intensity when the on-off keying of the pulses in the train is considered a source of coherent noise.¹¹ The results presented here are not exact but rely on a small-signal approximation of the jitter source. This technique has been widely applied in the analysis of the RF intensity spectrum of timing jitter noise in mode-locked lasers.^{12–15} Although much of our notation is inherited from these earlier papers, our results have a wider scope, because the only basic assumption is the coherence of the underlying optical carrier. Moreover, and in contrast to our previous time-domain

study¹⁰ in which independent pulse-to-pulse jitter variations were assumed, here arbitrary pulse-to-pulse timing jitter correlation is allowed.¹⁵

The plan of this paper is as follows: In Section 2 we analyze the power spectrum of the intensity of the jittery trains before and after the trains pass through a Talbot dispersive device. Details of the small-signal computation of the power spectral density are deferred to Appendix A. In Section 3 we present a number of examples of the intensity spectrum, targeted on 10-GHz trains. In Section 4 we numerically investigate the conditions for a decrease in the noise power around the harmonics. Finally, our conclusions and a discussion are presented in Section 5.

2. INTENSITY POWER SPECTRUM

The propagation of pulses carried by monochromatic light in guided dispersive media is modeled by use of a linear system. The pulse envelope, $E(z, t)$, propagates in the absence of attenuation and nonlinear effects according to the law¹⁶

$$\frac{\partial E}{\partial z} = -i \frac{\beta_2}{2} \frac{\partial^2 E}{\partial t^2}, \quad (1)$$

where $\beta(\omega) = \beta_0 + (\omega - \omega_0)\beta_1 + (\omega - \omega_0)^2\beta_2/2 + \dots$ is the expansion of the dispersion relation around optical carrier frequency ω_0 and t is the time measured in the proper frame of reference of the pulse, $t = t_{\text{phy}} - \beta_1 z$, where t_{phy} is the physical time. β_3 and other higher-order dispersion terms are not taken into account. The impulse response or propagation kernel of linear problem (1) is the one-dimensional Fresnel diffraction kernel. For a dispersive medium of length L , its transfer function is $H_\xi(\omega) = \exp(i\xi\omega^2/2)$, where $\xi = \beta_2 L$ is the accumulated dispersion of the line. Let us consider as input field envelope $E_0(t)$ a jittery train of Gaussian pulses:

$$\begin{aligned} E_0(t) &= \sum_k f(t - kt_0 - a_k) \\ &= \sum_k \exp[-(t - kt_0 - a_k)^2(1 + iC)/2t_p^2]. \end{aligned} \quad (2)$$

In Eq. (1), f is the pulse profile, which is assumed to be Gaussian and linearly chirped; C is the chirp parameter and t_p is its temporal width. Unless stated otherwise, sums and integrals run from $-\infty$ to $+\infty$. Timing jitter is modeled by use of an infinite collection of random variables¹⁵ a_k ($k = -\infty, \dots, +\infty$), so t_0 is the exact period of the train in the absence of jitter. This assumes that jitter does not alter the pulse profile. We also assume that the pulse widths are smaller than the exact period, $t_p < t_0$, in such a way that overlapping between Gaussian pulses in the input train can be neglected. Jitter variables a_k have zero mean and standard deviation σ_j , and the average over the values of a_k is denoted by brackets, $\langle \cdot \rangle$. Therefore $\langle a_m \rangle = 0$ and $\langle a_m^2 \rangle = \sigma_j^2$ for any pulse index m . Correlation between pulses, assumed stationary, is described by pulse-to-pulse timing jitter correlation function R , defined as $R(k) = R(-k) = \langle a_m a_{m \pm k} \rangle$.

The input envelope [Eq. (2)] is transformed by the linear system [Eq. (1)] into output envelope $E_\xi(t)$. The Fourier transforms of the input, $\hat{E}_0(\omega) = \int dt \exp(i\omega t)E_0(t)$, and the output, $\hat{E}_\xi(\omega)$, fields are related by

$$\begin{aligned} \hat{E}_\xi(\omega) &= H_\xi(\omega)\hat{E}_0(\omega) \\ &= t_p[2\pi/(1 + iC)]^{1/2} \exp(-\rho\omega^2/2) \\ &\quad \times \sum_k \exp(i\omega k t_0 + i\omega a_k), \end{aligned} \quad (3)$$

where we have introduced the notation $\rho = \tau^2 - i\xi - iC\tau^2$ and $1/\tau = (1 + C^2)^{1/2}/t_p$. The quantity $1/\tau$ is the linewidth of the pulses in the train. We assume that the standard deviation of timing jitter σ_j is much smaller than the inverse of the pulse's linewidth, $\sigma_j \ll \tau$. The approximate formulas for the power spectral density that we derive are based on a second-order expansion of σ_j/τ or, equivalently, on a small-signal approximation in the variables a_k .

The temporal Talbot effect arises when the absolute value of the accumulated dispersion of the line is an integer of the fractional multiple of a basic scale:

$$|\xi| = \frac{t_0^2}{2\pi} \frac{\gamma}{\alpha}, \quad (4)$$

where γ and α are positive and coprime integers. The effect consists of a formation of a replica of the original train when the ratio γ/α is an integer number ($\alpha = 1$) and of a more-complex periodic structure when this ratio is fractional. These two conditions lead to an integer or a fractional Talbot effect, respectively.¹⁷ We are interested only in the properties of integer Talbot-imagined trains, so we set $\alpha = 1$ in what follows.

The temporal properties of the integer Talbot-filtered trains can be described on the basis of Eq. (3) as follows: Let us consider nonjittery trains, i.e., $a_k = 0$, such that in Eq. (3) the spectral content is composed of frequencies $\omega = k\omega_f$, where $\omega_f = 2\pi/t_0$ is the fundamental harmonic of the train. Then, at those values of dispersion given by Eq. (4) with $\alpha = 1$, the transfer function reduces to $H_\xi(k\omega_f) = \exp(\pm i\pi\gamma k^2) = (-1)^{\gamma k}$. When γ is even, the integer Talbot filter is unity in the harmonics and thus leaves invariant the spectral components of the train. The Talbot replica is therefore a train composed of the same initial Gaussian and linearly chirped pulses. When γ is odd, the integer Talbot filter adds relative phase shift π between consecutive harmonics. The replica is also composed of the same initial Gaussian and linearly chirped pulses, now shifted by $t_0/2$ in the proper reference frame.

Notice from Eq. (3) that linear chirp and dispersion have similar functions, through the imaginary part of the ρ parameter. This means that in certain conditions a pulse sequence that results from a dispersive line is not necessarily a replica of the initial train. Let us consider a small deviation of dispersion from the design value, $\xi = \xi_D + \Delta\xi$, with $|\xi_D| = t_0^2\gamma/2\pi$ and $|\Delta\xi| \ll |\xi_D|$. Because of the cumulative effect of dispersion, the effect of this line over the initial train can be explained in a two-step way. The ξ_D portion of the line creates an exact rep-

lica of the train, composed of the original Gaussian and linearly chirped pulses, whereas the extra amount of dispersion $\Delta\xi$ compresses or broadens these pulses individually. The temporal width t_p' of the resultant pulses is¹⁶

$$t_p' = t_p \left[\frac{1 + (C + \Delta\xi/\tau^2)^2}{1 + C^2} \right]^{1/2}. \quad (5)$$

For instance, if an extra amount of dispersion is added or extracted such that $C + \Delta\xi/\tau^2 = 0$, the output pulses get compressed. This is the conventional method of pulse compression by a dispersive line, applied here to the output pulses of the train. In this paper, and to simplify our analysis, we take into consideration only exact Talbot values, i.e., values of the form $|\xi| = t_0^2\gamma/2\pi$, thus retaining parameter C as the true chirp of the pulses of the initial train and its replica. In any case, our formulas are suitable for the analysis of deviations of these values of dispersion according to the preceding discussion.

From these considerations it also follows that a Talbot filter is defined by its ability to introduce the appropriate spectral phases into the spectral content of a coherent train, through the imaginary part of the ρ parameter. The use of a dispersive line is the most obvious choice for performing this task, but any device designed to create the necessary phases would filter the train in the same way. For instance, pulse compression has been demonstrated without the use of a dispersive line together with the Talbot increase of the repetition rate of the sequence.^{18,19}

Inasmuch as dispersion is a phase-only filter, the temporal Talbot effect leaves invariant the power spectrum $|\hat{E}_0(\omega)|^2$ of the optical envelope, as measured in an optical spectrum analyzer.^{5,7} However, if detection occurs after the dispersive device, the photocurrent that is generated is proportional to the intensity, $I_\xi(t) = |E_\xi(t)|^2$, so dispersion-induced phases of the different spectral components of the train can distort the power spectrum of the detected train by multiple interference. The RF spectrum of the intensity is obtained from the Fourier transform of the mean correlator of intensities²⁰:

$$S_\xi(\omega) = \int_{-\infty}^{+\infty} d\tau \exp(i\omega\tau) \left[\lim_{T \rightarrow \infty} \frac{1}{2T} \int_{-T}^T dt \langle I_\xi(t + \tau) I_\xi(t) \rangle \right]. \quad (6)$$

The power spectral density of this dispersed train is composed of a signal manifested in the RF spectrum by harmonics at multiples of the fundamental frequency of the train, $\omega_f = 2\pi/t_0$, and a noise spectrum, $S_\xi^{(N)}(\omega)$. The main result of this paper is the analysis of the noise spectrum of the intensity, computed to second order in a_k . Its value is

$$t_0 S_\xi^{(N)}(\omega) \equiv \omega^2 J(\omega) \Phi(\omega) \sum_n G_n(\omega) M_n(\omega). \quad (7)$$

The details of the computation are presented in Appendix A. In formula (7) the power spectrum is composed of a sum of four types of contribution. The first one is a smooth broadband function, $\omega^2 J(\omega)$, which represents the envelope function of noise in the spectral domain that has bandwidth $1/\tau$.

$$\omega^2 J(\omega) = \pi t_p^2 \omega^2 \exp(-\omega^2 \tau^2 / 2). \quad (8)$$

The second function in formula (7), $\Phi(\omega)$, is the power spectrum of the timing jitter,¹⁵ which is the Fourier transform of the jitter correlation function:

$$\Phi(\omega) = \sum_k R(k) \exp(i\omega k t_0). \quad (9)$$

This function is manifestly ω_f periodic, and, in general, it is narrowband about the harmonics.^{12,15} However, in the noncorrelated timing noise limit, $R(k) = \sigma_j^2 \delta_{k0}$, the jitter noise becomes white, i.e., $\Phi(\omega) = \sigma_j^2$.

The terms in the sum in formula (7), however, are dispersion dependent and jitter independent. Each term in this sum is composed of a Gaussian function $G_n(\omega)$, to which we refer as the n spectral window, and an oscillatory function $M_n(\omega)$, to which we refer as the modulation function of the n window. The functions $G_n(\omega)$ account for the portions of noise at which the previous noise contributions, $\omega^2 J(\omega)$ and $\Phi(\omega)$, are damped, thus providing the mechanism of noise filtering by multiple interference. Their functional form is Gaussian:

$$G_n(\omega) = \exp[-(\omega\xi + \omega C\tau^2 - nt_0)^2 / (2\tau^2)]. \quad (10)$$

Finally, the functions $M_n(\omega)$ modulate the spectral windows $G_n(\omega)$ through a combination of oscillatory terms:

$$M_n(\omega) = [\cos(\omega n t_0 / 2) - (\xi + C\tau^2 - n t_0 / \omega) \times \sin(\omega n t_0 / 2) / \tau^2]^2. \quad (11)$$

These functions $M_n(\omega)$ are regular in the limit $\omega \rightarrow 0$.

To gain intuition into the formulas written above, let us consider the input-noise limit. This is the RF noise of the intensity of the train before it enters the dispersive line, measured by direct detection of the train with a high-bandwidth photodetector. We obtain it by setting $\xi = 0$ in expressions (7)–(11). First, notice that the spectral windows become centred at $\omega = n t_0 / |C| \tau^2$. Because $t_0 > \tau$ and the bandwidth of the spectrum of the individual pulses is of the order of $1/\tau$, the peak contribution of $G_n(\omega)$ when $n \neq 0$ lies outside the pulse spectrum. Therefore we neglect the contributions of all the spectral windows except that with index $n = 0$. In addition, the corresponding modulation function is unity, $M_0(\omega) = 1$, and thus the input noise spectrum reduces to

$$t_0 S_0^{(N)}(\omega) \equiv \omega^2 |F(\omega)|^2 \Phi(\omega), \quad (12)$$

where $|F(\omega)|^2 = \pi t_p^2 \omega^2 \exp(-\omega^2 t_p^2 / 2)$ is the spectrum of the intensity of a single pulse, $|f(t)|^2$. This formula is well known in the context of characterization of noise in fundamentally mode-locked lasers.^{12–15} Its interpretation is simple: Direct detection of the mistimed train [Eq. (3)] originates a jittery photocurrent proportional to the intensity, $I_0(t) \equiv \sum_k |f(t - k t_0 - a_k)|^2$, where we have neglected any pulse overlap in the sum. Then, by expanding this photocurrent linearly in the jitter variables, we recover the noise spectrum [formula (12)]. Thus direct detection of the original train misses the information on the phase of the pulses and is therefore independent of any phase modulation.

When a replica of the train is created after a Talbot dispersive line, the basic features of the noise spectrum are

similar to those found in the analysis of noise induced by on-off keying of an exact train.¹¹ First, the broadband envelope of the spectrum, $\omega^2 J(\omega)$, extends along the optical linewidth of a single pulse of the train such that, if the pulses are chirped, the noise bandwidth is broader than the bandwidth of the input noise envelope $\omega^2 |F(\omega)|^2$. Second, noise is filtered around the maxima of the spectral windows $G_n(\omega)$. These maxima are located at

$$\omega^{(n)} = \frac{nt_0}{|\xi + C\tau^2|} \cong \omega_f \frac{n}{\gamma} \left[1 - \text{sign}(\xi) \frac{2\pi C}{\gamma} \frac{\tau^2}{t_0^2} \right]. \quad (13)$$

According to formula (13), when the initial pulses are unchirped and spectral window index n is a multiple of γ , these windows are centered, like $\Phi(\omega)$, over the harmonics. When Talbot index γ is not unity, between two consecutive harmonics there are $\gamma - 1$ spectral windows uniformly separated. When the initial pulses are chirped there exists a deviation of the maxima of the spectral window functions $G_n(\omega)$ that depends on the relative sign between dispersion and chirp. When dispersion is positive, $\xi > 0$, the maxima [formula (13)] are redshifted (blue-shifted) if the chirp is positive (negative). The noise spectral window with index n will therefore exhibit a maximum in the neighborhood of a harmonic of the train when $n = h\gamma$, where h is the harmonic index. The noise maximum can be raised with respect to the noise value before dispersion. Nevertheless, the precise value of noise at the harmonic frequencies $h\omega_f$ does not change.

The full width of the 10-dB decay of these spectral windows is computed from Eq. (10), providing a simple estimate of the bandwidth of the resultant noise spectrum about the harmonics:

$$\Delta_W \omega = \frac{2\sqrt{2}}{\sqrt{\log_{10} e}} \frac{\tau}{|\xi + C\tau^2|} \cong 4.3 \frac{\tau}{|\xi|} = \frac{4.3}{t_0 Q}. \quad (14)$$

This width is common to all the spectral windows. In formula (14) we have defined parameter Q :

$$Q = \frac{\gamma}{2\pi} \frac{t_0}{\tau}. \quad (15)$$

Because the temporal width of a pulse after a dispersive line of high dispersion ξ goes as¹⁶ $t_0 Q$, Q is the temporal dispersion-induced spread of an individual pulse with respect to the pulse separation and represents the number of basic time periods of the original train that occupies a pulse after dispersion.

Finally, each of these spectral windows is modulated by the functions $M_n(\omega)$. In this case the structure of the modulation is richer than that found in the analysis of on-off-keyed trains after Talbot devices.¹¹ First, notice that on the top of the spectral windows that correspond to output harmonics ($n = h\gamma$) the value of $M_n(\omega)$ is unity, showing ripples as the offset from the top increases. When the spectral window index does not correspond to an output harmonic, however, the modulation function does not reach a local maximum on top of the windows. Then these windows show tips on top that are due to this nonmaximal modulation. Moreover, modulation maxima

are in general bigger than unity, so noise can rise above the broadband envelope [Eq. (8)]. We present an example of this property in Section 3 below.

Noise vanishes when modulation reaches zero, $M_n(\omega) = 0$; near the n window that corresponds to the h harmonic, the equation $M_n(\omega) = 0$ can be represented by means of a variable x that accounts for the offset from the value of the harmonic, $\omega(x) = \omega_f(h + x)$. Then the zeros of the modulation are the solutions of

$$\cot(\pi h \gamma x) = \text{sign}(\xi) C + \frac{2\pi Q^2}{\gamma} \frac{x}{x + h}. \quad (16)$$

A graphic analysis of this function shows that there exist two different sets of solutions, which correspond to equal numbers of positive and negative values of x . There exists a zero in each incremental offset of width ω_f/n on the left and the right sides of the harmonics that correspond to the branches of the cotangent function. The location of the zeros is not exactly symmetric with respect to the harmonic, even in the absence of chirp. Therefore, noise skirts around harmonics will always be asymmetric. Because of the decreasing character of the branches of the cotangent function, when both chirp and dispersion have the same sign the zeros of modulation are located at lower values of the offset than those with unchirped pulses. If chirp and dispersion have different signs, the offset of the zeros increases. For large values of Q the two sets of left and right solutions approximate the solutions of $\tan(\pi h \gamma x) = 0$. These properties are also exemplified and analyzed in the Section 3.

3. EXAMPLES OF THE POWER SPECTRUM

To present examples of the power spectrum it is necessary to introduce a concrete model for the correlation between pulses. It is not our objective to review the possible characteristics of noise and its origin. They ultimately depend on the concrete systems that generate the trains. Here we use a simple model derived from the noise theory of fundamentally mode-locked lasers,¹⁵ which permits a general illustration of the traces in the intensity spectrum by consideration of different types of pulse-to-pulse timing jitter correlation.

We assume that jitter is correlated through a recursive relation between adjacent pulses. The deviation of the center of the pulses is a fraction $\eta > 0$ of the deviation of the previous pulse, augmented by an additional term ϵ_m :

$$a_m = \eta a_{m-1} + \epsilon_m. \quad (17)$$

It is assumed that both quantities have zero mean, $\langle a_m \rangle = \langle \epsilon_m \rangle = 0$, and that the additional terms are mutually independent and thus uncorrelated, $\langle \epsilon_m \epsilon_n \rangle = T^2 \delta_{mn}$. Therefore η controls the correlation between pulses and depends on the underlying mechanism of pulse generation. The jitter variations described by parameter ϵ_m , however, represent noise induced by spontaneous emission or vacuum fluctuations.

The relation of the two parameters, η and T , to the rms value of jitter is $T^2 = \sigma_j^2(1 - \eta^2)$. The correlation function is $R(k) = \sigma_j^2 \eta^{|k|}$. Thus jitter noise is uncorrelated and therefore white when $\eta = 0$, whereas totally corre-

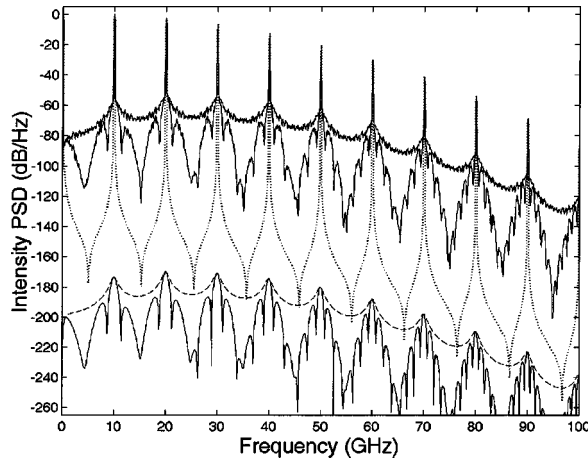


Fig. 1. Intensity power spectral density (PSD) of a jittery train of pulses ($\sigma_j = 100$ fs, $\eta = 0.7$) before and after a temporal Talbot device with index $\gamma = 1$. Pulse width, $t_p = 10$ ps; chirp, $C = 0$; repetition rate, 10 GHz; $Q = 1.59$. Above, numerical power spectral densities for the input and output trains (continuous curves) and numerical power spectral density of the mean signal (dotted curve). Below, analytical noise power spectral densities for the input (dashed curve) and output (continuous curve) trains.

lated noise corresponds to $\eta = 1$. The timing jitter's spectral density is straightforwardly computed from the correlation, resulting in a Fabry–Perot-type function:

$$\Phi(\omega) = \sigma_j^2 \frac{1 - \eta^2}{1 - 2\eta \cos(\omega t_0) + \eta^2}. \quad (18)$$

Notice that this function is manifestly periodic, with a period equal to the fundamental harmonic of the train, and is peaked in the harmonics. Thus the noise spectrum's density before it enters the Talbot dispersive line has symmetric noise RF sidebands or skirts around each harmonic. Expansion of Eq. (18) around a harmonic $h\omega_f$ reduces the form of the skirts to a Lorentzian shape.¹⁵

In all the examples presented in this section the pulse-to-pulse-temporal separation is $t_0 = 100$ ps, corresponding to trains with repetition rate $\omega_f = 2\pi \times 10$ GHz. The temporal width of the pulses in the train is $t_p = 10$ ps, and the jitter's standard deviation is $\sigma_j = 100$ fs. The simulations presented here were generated from a string of 1024 basic periods, each with 64 sample points. The power spectrum is estimated numerically by use of the Bartlett algorithm,²¹ averaging 8 spectra, each obtained from a sequence of 128 time periods. The frequency separation of the points in the spectrum is therefore 78 MHz ($=1/128 \times 100$ ps). Jitter is created numerically by use of standard pseudorandom number generators and recursive relation (17).

In Fig. 1 we represent the spectrum of a train of unchirped pulses ($C = 0$) that corresponds to the intensity of the jittery train before and after the Talbot dispersive line. Dispersion is adjusted to create the first integer Talbot image of the original train ($\gamma = 1$), so $Q = 1.59$. The parameter that describes correlation is $\eta = 0.7$. In the lower part of Fig. 1 we represent by a dashed curve our analytical approximation of the noise spectral power of the detected train before it enters this dispersive de-

vice, as given by formula (12). By a continuous curve we plot analytical formula (7) of the noise spectral power of same train detected after the Talbot device. In the upper part of the figure we depict the simulation of the spectra before and after the Talbot dispersive line, normalizing the dc component to 0 dB. These spectra show peaked contributions that correspond to the harmonics of a perfect train. To help in visualizing the contributions of noise we represent the spectrum of the mean signal by using a dotted curve. The agreement between simulations and analytical formulas is excellent.

To appreciate the different contributions to the RF noise skirts around the harmonics, we plot in Fig. 2 the contributions to noise in the right-hand offset near 50 GHz. The offset runs up to 5 GHz, the midpoint between harmonics. At the left in Fig. 2, and normalizing the power spectrum to 0 dB at zero offset, we represent jitter power spectrum $\Phi(\omega)$ by using a dashed curve, modulation function $M_{n=5}(\omega)$ by using a continuous curve, and window function $G_{n=5}(\omega)$ with a dotted curve. The different contributions to the total power spectrum are clearly observed. The jitter power spectrum has a 10-dB half-width of 1.71 GHz; the 10-dB decay half-width of spectral window function $G_{n=5}(\omega)$ is 2.15 GHz. Modulation function $M_{n=5}(\omega)$ provides an additional structure to the resultant right-hand noise skirt. The product of these contributions is depicted at the right in Fig. 2 by continuous curve, together with the contributions of the window function and the jitter power spectrum for comparison. Notice that the global 10-dB decay half-width has been reduced to less than 600 MHz.

The locations of the zeros of the modulation in Fig. 2 were obtained by numerical integration of Eq. (16). In Fig. 3 we present the positions of the offset that correspond to the zeros as a function of parameter Q for the fifth harmonic ($h = 5$), and the first integer Talbot device ($\gamma = 1$), for three values of the pulse chirp: $C = 0$ (continuous curves), $C = 1$ (dashed curves), and $C = -1$

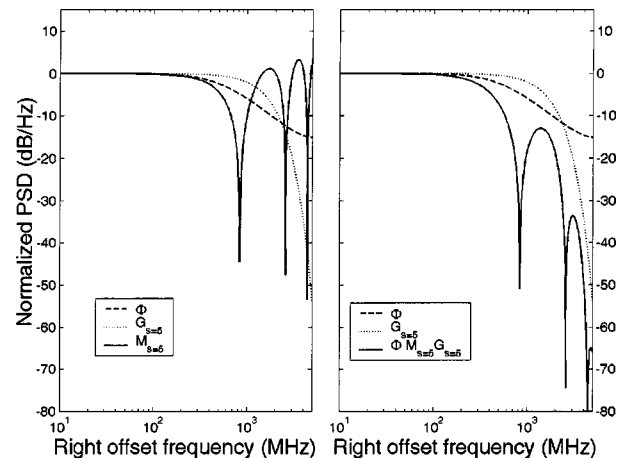


Fig. 2. Contributions to the right-hand offset noise spectrum of the train in Fig. 1 near the fifth harmonic ($n = h = 5$). Left, dashed curve, jitter power spectrum $\Phi(\omega)$; dotted curve, spectral window function $G_{n=5}(\omega)$; continuous curve, modulation function $M_{n=5}(\omega)$. Right, dashed curve, jitter power spectrum $\Phi(\omega)$; dotted curve, spectral window function $G_{n=5}(\omega)$; continuous curve, product $\Phi(\omega)G_{n=5}(\omega)M_{n=5}(\omega)$. PSD, power spectral density.

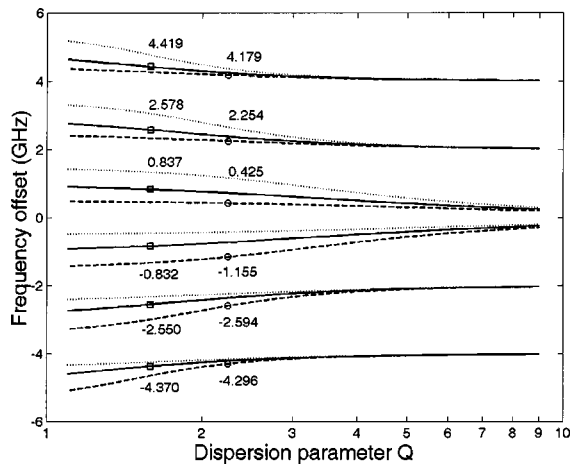


Fig. 3. Frequency offsets corresponding to the location of the zeros of the modulation function for the fifth harmonic ($h = 5$) and the first integer Talbot replica ($\gamma = 1$). Chirp: $C = 0$, continuous curves; $C = 1$, dashed curves; $C = -1$, dotted curves.

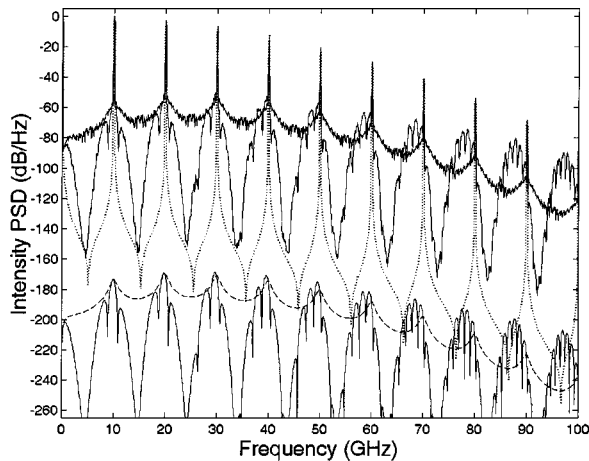


Fig. 4. Intensity power spectral density (PSD) of a jittery train of pulses ($\sigma_j = 100$ fs, $\eta = 0.7$) before and after a temporal Talbot device with index with $\gamma = 1$. Pulse width, $t_p = 10$ ps, chirp, $C = 1$; repetition rate, 10 GHz; $Q = 2.25$. Above, numerical power spectral densities for the input and output trains (continuous curves) and numerical power spectral density of the mean signal (dotted curve). Below, analytical noise power spectral densities for the input (dashed curve) and output (continuous curve) trains.

(dotted curves). There are six zeros in the offset range from -6 to 6 GHz, three on each side, and each in an incremental offset of 2 GHz. As dispersion is positive, positive chirp lowers the offset, whereas negative chirp raises it. Notice also that the zeros of the modulation tend to the roots of the tangent for high values of Q , as anticipated from the structure of Eq. (16). In Figs. 1 and 2 the value of parameter Q is 1.59. The corresponding zeros and their offset values are marked by open squares in Fig. 3, in agreement with our simulation of Fig. 1.

In Fig. 4 we present, following the same conventions as above, a 10-GHz train composed of Gaussian pulses, also with width $t_p = 10$ ps and $\eta = 0.7$ but now chirped with $C = 1$ ($Q = 2.25$). The centers of the spectral windows are redshifted owing to chirp. This asymmetry, together with the modulation, result in a globally asymmetric

noise pattern. Moreover, after the fifth harmonic the noise after the Talbot device is greater than noise before the Talbot device in the left-hand offset region. To illustrate the noise sidebands of the fifth harmonic, we plot in Fig. 5 the left and right noise skirts up to offsets of ± 5 GHz, where the asymmetry of the output noise is apparent. With a dashed curve we present the jitter's power spectral density $\Phi(\omega)$ [Eq. (18)]. The output-noise approximation [formula (7)], is represented by a continuous curve. We subtracted from this last spectrum the input noise envelope $\pi t_p^2 \omega^2 \exp(-\omega^2 t_p^2/2)$, such that the represented function coincides with the product $\Phi(\omega)G_{n=5}(\omega)M_{n=5}(\omega)$. Dots for the input and crosses for the output are superimposed upon the numerical data taken from Fig. 4. We have avoided the use of points with offsets below 100 MHz because they overlap the peaks that represent the harmonics. The zeros of the output noise as well as their numerical values were depicted previously by circles in Fig. 3.

Finally, in Figs. 6 and 7 we present a new example of a power spectrum that corresponds to the replica of a 10-GHz train in the second integer Talbot dispersive device, $\gamma = 2$, composed of unchirped pulses $C = 0$ of width $t_p = 10$ ps, such that $Q = 3.18$. Timing jitter is added, with $\eta = 0.5$. In Fig. 6 we show the overall form of the spectrum, which presents new spectral windows between consecutive harmonics. Notice the elevation above the broadband noise envelope of the first spectral window at 5 GHz that is due to the modulation. Figure 7 corresponds to a double logarithmic plot of the noise skirts around the fifth harmonic (tenth spectral window). We plotted the analytical continuous curve by taking into account only the tenth window. Therefore, at the left and right sides of this plot, below -2.5 GHz and above 2.5 GHz, the numerical data of the output noise correspond to portions of the ninth and eleventh spectral windows, which are centered at 45 and 55 GHz, respectively. Using Eq. (16), we computed the zeros of the modulation of the central window; the values of the offsets are 2204, 1286, 418, -417 , -1278 , and -2191 MHz, in agreement with the locations in Fig. 7.

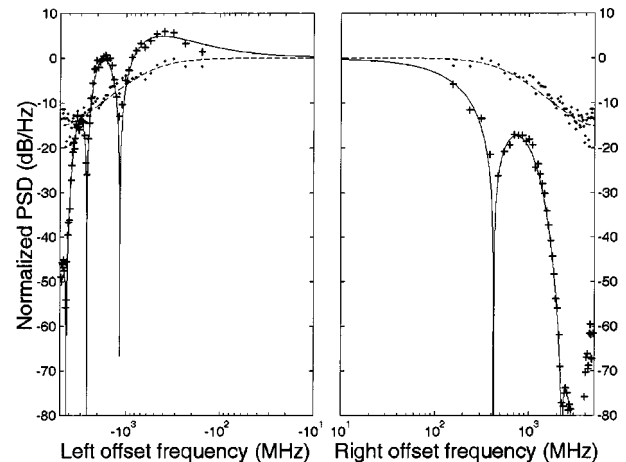


Fig. 5. Left and right offset noise power spectra of the train of Fig. 4 around the fifth harmonic ($n = h = 5$). Dashed curves, analytical input noise power spectral density (PSD). Continuous curves, analytical output noise power spectral density. Numerical data extracted from Fig. 4 superimposed: dots, input noise; crosses, output noise.

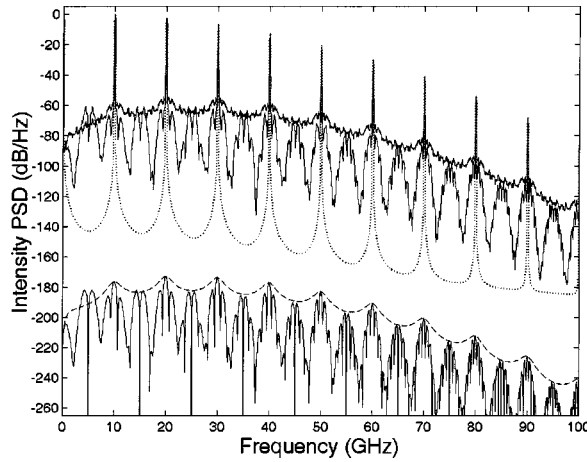


Fig. 6. Intensity power spectral density (PSD) of a jittery train of pulses ($\sigma_j = 100$ fs, $\eta = 0.5$) before and after a temporal Talbot device with index $\gamma = 2$. Pulse width, $t_p = 10$ ps; chirp, $C = 1$; repetition rate, 10 GHz; $Q = 3.18$. Above, numerical power-spectral densities for the input and output trains (continuous curves), and numerical power spectral density of the mean signal (dotted curve). Below, analytical noise power spectral densities for the input (dashed curve) and output (continuous curve) trains.

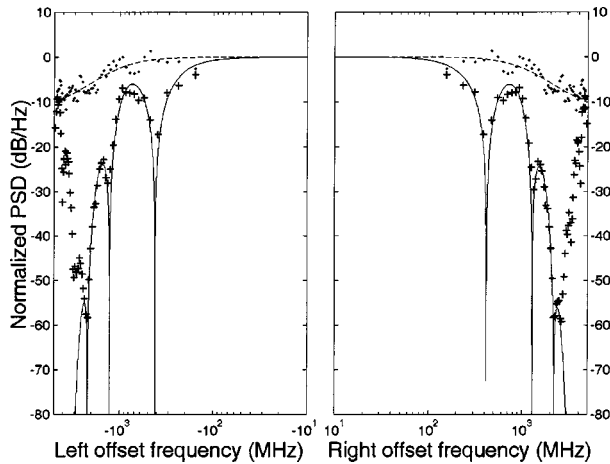


Fig. 7. Left and right offset noise power spectra of the train of Fig. 6 around the fifth harmonic ($h = 5$, $n = 10$). Dashed curves, analytical input noise power spectral density (PSD). Continuous curves, analytical output noise power spectral density. Numerical data extracted from Fig. 6 superimposed: dots, input noise; crosses, output noise.

4. JITTER SMOOTHING

The integration of the RF noise skirts in a symmetric domain of bandwidth ω_f about the h th harmonic is one of the standard operational tools used to obtain experimentally the rms value of the timing jitter of a train from noise analysis of the intensity before it passes through a dispersive line.¹² The procedure that permits a simple determination of jitter is to approximate the broadband noise envelope in formula (12) by its value in the harmonic and to integrate along a passband of width ω_f about the harmonic. This renders the total integrated noise proportional both to squared harmonic index h^2 and to standard deviation σ_j^2 of the rms jitter:

$$\begin{aligned} & \int_{(h-1/2)\omega_f}^{(h+1/2)\omega_f} d\omega S_0^{(N)}(\omega) \\ & \cong t_0^{-1} \omega_f^2 h^2 |F(h\omega_f)|^2 \int_{(h-1/2)\omega_f}^{(h+1/2)\omega_f} d\omega \Phi(\omega) \\ & = t_0^{-1} \omega_f^3 h^2 |F(h\omega_f)|^2 \sigma_j^2. \end{aligned} \quad (19)$$

Then, from a comparative measurement of different integrated RF noise sidebands, the value of rms jitter is experimentally determined.

As we illustrated in Section 3, the RF noise skirts after a Talbot dispersive line change as a result of to the presence of the spectral windows and the modulation functions. Thus total noise, measured as the result of integration of the noise skirt spectrum along a passband around the harmonics, can get smoothed. Notice that, because of the structure of the noise skirts after the Talbot dispersive line, the output noise cannot be ascribed to the timing jitter of the output train. The interpretation of output noise as a specific combination of both amplitude and timing jitters in the pulses of the output train will not be addressed in this paper.

The integrated noise along bandwidth ω_f about the h th harmonic after the Talbot dispersive line is expressed as

$$\begin{aligned} & \int_{(h-1/2)\omega_f}^{(h+1/2)\omega_f} d\omega S_{\xi}^{(N)}(\omega) \\ & \cong t_0^{-1} \omega_f^2 h^2 J(h\omega_f) \\ & \quad \times \int_{(h-1/2)\omega_f}^{(h+1/2)\omega_f} d\omega \Phi(\omega) G_{n=h\gamma}(\omega) M_{n=h\gamma}(\omega). \end{aligned} \quad (20)$$

In formula (20) we have also approximated the broadband envelope by its value in the harmonic and have retained in the sum only the spectral window that corresponds to the harmonic, $n = h\gamma$. According to the examples presented in Section 4, this is a good approximation when the dispersive line is adjusted to the first integer Talbot image, $\gamma = 1$, because no new spectral windows between harmonics appear in the spectrum. The extension of the integration to a bigger number of windows is nevertheless straightforward.

Then the ratio $\rho^{(h)}$ of the integrated RF noise power after dispersion [formula (20)] to that before dispersion [formula (19)] is expressed, from formulas (7)–(12), as

$$\rho^{(h)} \cong \exp[n^2 C^2 / (2Q^2)] L_{n=h\gamma}(\eta, Q, C), \quad (21)$$

where the first term accounts for the different noise envelopes and

$$L_{n=h\gamma}(\eta, Q, C) = \int_{-1/2}^{1/2} dx \bar{\Phi}(x) G_{n=h\gamma}(x) M_{n=h\gamma}(x). \quad (22)$$

In Eq. (22) we perform the integration by again using the variable $\omega(x) = \omega_f(h + x)$ and with the notation $\bar{\Phi}(x) \equiv \Phi[\omega(x)]/\sigma_j^2$, $G_{n=h\gamma}(x) \equiv G_{n=h\gamma}[\omega(x)]$, and $M_{n=h\gamma}(x) \equiv M_{n=h\gamma}[\omega(x)]$.

From the structure of formula (21) the following consequences are derived: First, the ratio in formula (21) depends on correlation, not on the precise value of σ_j^2 . Second, if pulses are unchirped, noise is essentially

symmetric about the harmonic, and the resultant ratio is always less than unity because of the presence of the spectral window. The reduction increases as the width of the window narrows, so smoothing increases with Q and also as $\eta \rightarrow 0$, because the input noise is white in a bigger band. Finally, when the pulses are chirped the value of the ratio is raised through the exponential factor in formula (21) that accounts for the different noise envelopes. This increase becomes bigger at high harmonics.

In Fig. 8 we plot the ratio $\rho^{(h)}$ of the fifth harmonic ($h = 5$) of the first integer Talbot dispersive device ($\gamma = 1$) to correlation parameter η and for three values of Q . The values of the ratio [formula (21)] were obtained by numerical integration of Eq. (22). First, notice that, owing to the quadratic dependence of the integrated noise power [formula (19)] on the jitter's standard deviation σ_j , a reduction of 10 dB in the ratio $\rho^{(h)}$ amounts to a reduction of σ_j by a factor of 3, whereas a 6-dB decay is associated with a reduction of σ_j by a factor of 2. In Fig. 8(a) the ratio is computed for an initial train composed of unchirped pulses, whereas in Fig. 8(b) the pulses are slightly chirped ($C = 0.5$). As the correlation parameter controls the white-noise bandwidth of the RF noise skirts of the harmonic, this is one of the most determinant parameters of the smoothing; see Fig. 8(a). For high values of η , noise is correlated, the noise skirts are narrow, and consequently the noise reduction induced by the presence of the spectral windows is small. However, when the correlation is low, the presence of the windows induces a significant decrease in the RF noise skirts, which increases with parameter Q . Chirp is the most deleterious factor for this smoothing. From Figs. 4 and 5, when pulses are chirped the noise skirts are asymmetric and the peak values are raised above the initial noise level, leading to the increase in the ratio in formula (21) illustrated in Fig. 8(b). However, even in the presence of chirp, the combined effect of high Q and low correlation can lead to a significant decrease in the ratio $\rho^{(h)}$.

To visualize its dependence on the Q factor, and also its small variations within harmonic index h , in Fig. 9 we represent again the ratio for the first integer Talbot rep-

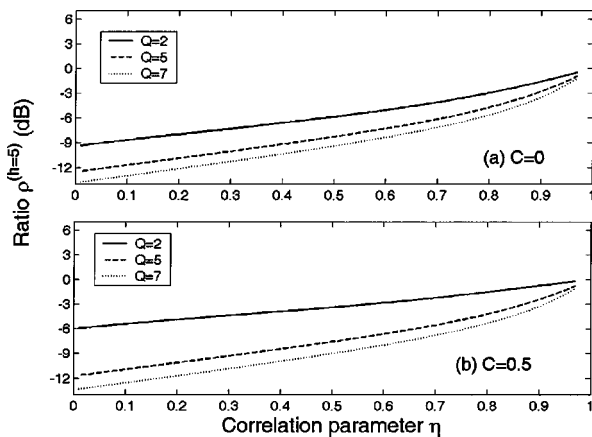


Fig. 8. Ratio $\rho^{(h)}$ for the fifth harmonic $h = 5$ (fifth spectral window, $n = 5$) and for the first integer Talbot replica $\gamma = 1$ as a function of correlation parameter η for three values of dispersion parameter Q : continuous curves, $Q = 2$; dashed curves, $Q = 5$; dotted curves $Q = 7$.

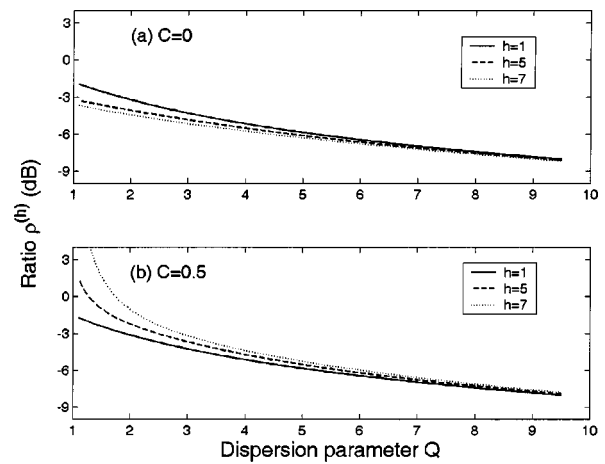


Fig. 9. Ratio $\rho^{(h)}$ for the first integer Talbot replica $\gamma = 1$ and for jittery trains with correlation parameter $\eta = 0.7$ as a function of dispersion parameter Q for three harmonics h : continuous curves, $h = 1$; dashed curves, $h = 5$; dotted curves, $h = 7$.

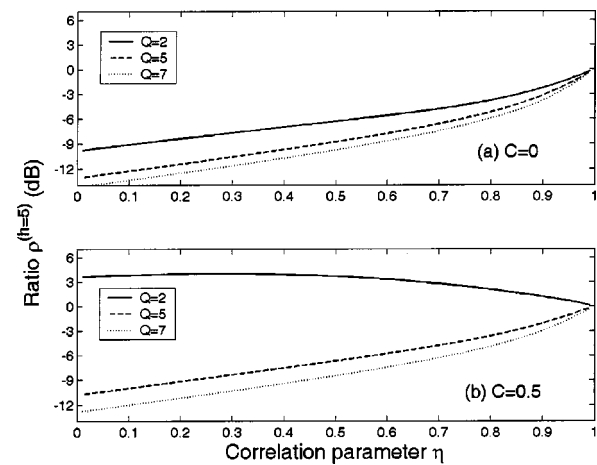


Fig. 10. Ratio $\rho^{(h)}$ for the fifth harmonic $h = 5$ (tenth spectral window, $n = 10$) and for the second integer Talbot replica $\gamma = 2$ as a function of correlation parameter η for three values of dispersion parameter Q : continuous curves, $Q = 2$; dashed curves, $Q = 5$; dotted curves, $Q = 7$.

lica, $\gamma = 1$, for jittery trains with correlation parameter $\eta = 0.7$ as a function of Q for different harmonics h and for the same two values of chirp, $C = 0$ and $C = 0.5$. Both the decrease in the ratio $\rho^{(h)}$ with Q and its small dependence on the harmonic are observed. Again, small chirps in Fig. 9(b) spoil the noise reduction. This effect is more pronounced for high harmonics, because the window shift and the subsequent increase in the noise peak value are proportional to the harmonic frequency. But notice that this increase in ratio $\rho^{(h)}$ for chirped pulses can be compensated for by means of an increase in Q .

In Figs. 10 and 11 we represent the ratio $\rho^{(h)}$ in the second Talbot device, $\gamma = 2$. The presence of new spectral windows between harmonics has been taken into account in the numerical evaluation of integral equation (22). In Fig. 10 we plot ratio $\rho^{(h)}$ for the fifth output harmonic, $h = 5$, with respect to the correlation parameter for different values of C and Q . When $C = 0$, the curves in Fig. 10(a) are similar to those in Fig. 8(a), proving that the ra-

tio depends basically on the value of Q through the width of the spectral window located in the harmonic. The presence of new windows adds a subsidiary contribution to ratio $\rho^{(h)}$. Therefore the increase in Talbot order produces an increase in the reduction of smoothing. However, when the chirp is nonzero, the subsequent change in the window position always increases the value of the ratio. In Fig. 10(b) the ratio becomes bigger than unity for low values of Q , but, again, increasing the value of Q compensates for the increase in the ratio.

Finally, in Fig. 11 we depict the evolution of ratio $\rho^{(h)}$ for the second integer Talbot replica, $\gamma = 2$, for jittery trains with correlation parameter $\eta = 0.7$, as a function of Q for three harmonics h . In Fig. 11(a), unchirped pulses are considered. These curves are similar to those of Fig. 9(a) except for the first harmonic, $h = 1$, whose values of the reduction are worse because of the presence of the new window at 5 GHz; Fig. 6. In Fig. 11(b) we consider chirped $C = 0.5$ pulses. Again, ratio $\rho^{(h)}$ increases owing to a shift in the window maximum and can be compensated for by use of high values of Q .

5. CONCLUSIONS AND DISCUSSION

In this paper we have presented a theoretical study of the RF spectral noise content of the intensity of a coherent jittery train of pulses after an integer Talbot dispersive line. We derived the power spectral density of the intensity in the small-signal approximation, assuming a general form of the timing jitter correlation between pulses and the coherence of the underlying pulse carrier. The spectrum has been exemplified through simulations. The basic feature of the resultant spectrum is the presence of a broadband noise-filtering mechanism by multiple interference at the scales of a fraction of the train's repetition rate, which provides a reduction of the integrated noise power around the harmonics as measured in the RF regime. The influence of chirp and optical linewidth of the individual pulses in the train was also analyzed.

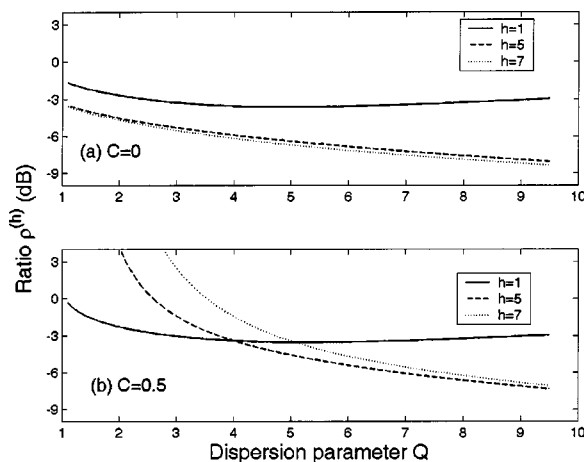


Fig. 11. Ratio $\rho^{(h)}$ for the second integer Talbot replica $\gamma = 2$ and for jittery trains with correlation parameter $\eta = 0.7$ as a function of dispersion parameter Q for three harmonics h : continuous curves, $h = 1$; dashed curves, $h = 5$; dotted curves, $h = 7$.

We have used the results derived to explore the noise reduction of different coherent Talbot-imagined trains under different propagation conditions. The smoothing of jitter noise by Talbot interference depends basically on the chirp of the pulses of the train, on the correlation between adjacent pulses in the train, and on the accumulated dispersion of the line but not on the absolute value of the timing jitter's standard deviation. Chirp has been shown to be the most deleterious factor because it induces a shift of the peak noise level with respect to the position of the harmonic that causes an increase in the total noise power. However, careful design of the dispersive line can easily compensate for it^{18,22} and compress the pulses simultaneously.

As correlation controls the jitter noise bandwidth before the jitter noise enters the dispersive line and because jitter smoothing is more pronounced at scales of the order of the repetition rate (typically less than 1 GHz for the 10-GHz trains), the initial noise must be broadband to produce significant jitter reduction. This fact limits the possible application of this procedure to trains composed of slightly correlated pulses. Ultimately, this application depends on the mechanisms that produce the trains. For instance, the use of a Talbot dispersive line cannot be successfully applied in fundamentally mode-locked lasers that have noise offsets up to 100 MHz; see, e.g., Ref. 14. In this case the active locking in the cavity of the laser produces highly correlated timing jitter. However, even in these cases the Talbot replica of a mode-locked laser output can in principle help to reduce other types of non-narrowband noise, such as the supermode noise²³ in harmonically mode locked lasers, for which both phase noise and timing jitter are uncorrelated between adjacent pulses.^{14,15}

The noise reduction depends on the accumulated dispersion of the line through the order of the Talbot replica. Basically, high Talbot orders imply the appearance of new noise windows between harmonics and the narrowing of the spectral window widths, which provides the bandwidth of the smoothed spectrum about the harmonics. Except for the first harmonic, the presence of new windows is a subsidiary effect when one is computing the decrease in noise ratio $\rho^{(h)}$. The narrowing of the spectral windows is controlled by dispersion parameter Q , which accounts for the width of the dispersed pulses relative to the repetition rate of the train. High Q values imply that the resultant pulses in a Talbot replica are formed from contributions of a high number of dispersed pulses, thus providing a coherently averaged output. The same smoothing mechanism has been found in the time domain.¹⁰

Finally, let us comment on the practical restrictions on the use of Talbot filters to treat jittery trains as described in this paper. The first limitation is the necessity for using linear filters with an exact or an approximately quadratic spectral phase over a sufficient bandwidth to cope with the optical bandwidth of the incoming train. This in practice imposes a limit on the temporal width of the pulses of the train. The second limitation is the accuracy of the total dispersion of the filter. As was noted in Section 2, a small deviation of dispersion causes temporal compression or broadening of the output pulses. Disper-

sion deviation is more deleterious in fractional Talbot filters because additional pulse broadening can cause interference between consecutive pulses; see Ref. 24 for a discussion. The integer Talbot filters analyzed here should show more tolerance to average dispersion deviations.

The third limitation is due to corrections in the spectral phase profile of the dispersive line. When prisms pairs, gratings pairs, or fibers (standard, dispersion-compensating, or dispersion-shifted) are used, the spectral phases suffers from (smooth) higher-order deviations of the quadratic behavior. If these higher-order corrections are negligible over the entire optical bandwidth of the train, the results presented here will still be applicable. In the case of dispersive lines based on fibers, deviations are more pronounced for long fiber lengths.²⁵ If deviations are not negligible, higher-order dispersion produces temporal ripplelike distortion in the expected output Gaussian pulse profile.²⁶ This distortion is manifested in the RF spectrum as deviations in the harmonics of higher order.

Another method of producing dispersive filters is the use of fiber Bragg gratings or other microstructured devices. In these filters a dispersion ripple is the main deviation of the spectral quadratic behavior. Dispersion ripples cause satellite pulses in the output,²⁷ which when they interfere with the other coherent pulses of the train cause amplitude noise. Noninterfering satellite pulses, associated with high ripple frequencies, reflect again in the high-frequency portion of the RF spectrum. Ripple frequencies of the order of the repetition rate's frequency cause the amplitude noise of the output.

Notice finally that a jittery train [Eq. (3)] contains in principle all the optical frequencies, not merely the harmonics associated with an exact nonjittery train. The smoothing mechanism presented here is the result of the damping of nonharmonic frequencies as the result of destructive interference after dispersion. If the filter is designed to reproduce the quadratic spectral phases at the harmonics of the exact train and to add other types of spectral phases to the remaining frequencies,¹⁹ a similar smoothing mechanism could take place. However, the spectral RF patterns presented here would not be applicable, because in deriving them we assumed a global quadratic behavior.

APPENDIX A: COMPUTATION OF THE INTENSITY SPECTRUM

The computation of Eq. (6) was performed in Fourier space. The correlator is expressed as

$$\langle I_{\xi}(t)I_{\xi}(t') \rangle = \int \int \frac{d\omega_1}{2\pi} \frac{d\omega_2}{2\pi} \exp[-i(\omega_1 t - \omega_2 t')] \times \langle \hat{I}_{\xi}(\omega_1) \hat{I}_{\xi}^*(\omega_2) \rangle, \quad (\text{A1})$$

where the Fourier intensity is the autocorrelation of the Fourier optical envelope:

$$\begin{aligned} \hat{I}_{\xi}(\omega) &= \int dt \exp(i\omega t) I_{\xi}(t) \\ &= \int \frac{d\omega'}{2\pi} \hat{E}_{\xi}(\omega + \omega') \hat{E}_{\xi}^*(\omega')^*. \end{aligned} \quad (\text{A2})$$

Let us suppose that the Fourier correlator in Eq. (A1) has the following form:

$$\begin{aligned} \langle \hat{I}_{\xi}(\omega_1) \hat{I}_{\xi}^*(\omega_2) \rangle &= \langle \hat{I}_{\xi}(\omega_1) \rangle \langle \hat{I}_{\xi}^*(\omega_2) \rangle + 2\pi K(\omega_1, \omega_2) \\ &\times \sum_s \delta(\omega_1 - \omega_2 - 2\pi s/t_0). \end{aligned} \quad (\text{A3})$$

Then, using Eqs. (6) and (A1), we can straightforwardly show that the noise spectral density is the diagonal part of regular function K : $S_{\xi}^{(N)}(\omega) = K(\omega, \omega)$. Thus the problem of computing $S_{\xi}^{(N)}(\omega)$ reduces to computation of the Fourier-domain correlator and the mean Fourier intensity. Using Eqs. (3) and (A2) yields the photocurrent by Gaussian integration. Introducing the notation $\mu_m(\omega) = (\omega\rho + imt_0)/(2\tau^2)$ results in

$$\begin{aligned} \hat{I}_{\xi}(\omega) &= t_p \sqrt{\pi} \exp(-\rho\omega^2/2) \sum_{pk} \exp(i\omega kt_0 + \tau^2 \mu_{p-k}^2 \\ &+ i\mu_{p-k}^* a_k + i\mu_{p-k} a_p) \\ &\times \exp[-(a_p - a_k)^2/(4\tau^2)]. \end{aligned} \quad (\text{A4})$$

Now we substitute Eq. (A4) into Eq. (A3) and expand the exponentials in Eq. (A4) to second order in jitter variables a_k , performing the expectation values according to our assumptions after Eq. (2). The result is proportional to the correlation of timing jitter variables:

$$\begin{aligned} \langle \hat{I}_{\xi}(\omega_1) \hat{I}_{\xi}^*(\omega_2) \rangle &= \langle \hat{I}_{\xi}(\omega_1) \rangle \langle \hat{I}_{\xi}^*(\omega_2) \rangle + \pi t_p^2 \exp(-\rho\omega_1^2/2 \\ &- \rho^* \omega_2^2/2) \sum_k \exp[i(\omega_1 - \omega_2)kt_0] \\ &\times \sum_{rsq} \exp[i\omega_2 qt_0] \\ &\times \exp[\tau^2(\mu_r^2 + \mu_s^*)^2] \\ &\times [\mu_s^* \mu_r R(q - s + r) \\ &+ \mu_r^* \mu_s^* R(q - s) + \mu_s \mu_r^* R(q) \\ &+ \mu_r \mu_s R(q + r)], \end{aligned} \quad (\text{A5})$$

where μ_r is evaluated at ω_1 and μ_s at ω_2 . From Eq. (A5) the diagonal part of function K can be directly read. To simplify its expression, a second approximation is necessary. Notice that in Eq. (A5) $|\exp[\tau^2 \mu_r^2(\omega)]| = \exp(\omega^2 \tau^2/4) G_r(\omega)^{1/2}$, where the functions $G_r(\omega)$ are defined in Eq. (10). Because these functions are narrow-band, the second approximation is to neglect their spectral overlapping. Then $\exp[\tau^2(\mu_r^2 + \mu_s^*)^2] \cong \exp(\omega^2 \tau^2/2) G_r(\omega) \delta_{rs}$, and substitution into Eq. (A5) yields

$$\begin{aligned} t_0 S_{\xi}^{(N)}(\omega) &\cong J(\omega) \sum_n G_n(\omega) \sum_q \exp(i\omega qt_0) [2|\mu_n|^2 R(q) \\ &+ \mu_n^*{}^2 R(q - n) + \mu_n^2 R(q + n)], \end{aligned} \quad (\text{A6})$$

where all the μ variables are now evaluated at ω . Finally, reordering the sums over q and using the definition of μ_r , and also definitions (9) and (11) yield formula (7).

ACKNOWLEDGMENTS

This study has been supported by the Ministerio de Educación y Ciencia, Spain, under project TIC2003-03041. The Grupo de Óptica GRIN at the Universidade de Santiago de Compostela is a Network of Excellence on Micro-Optics–European Union partner. L. Chantada is also supported by the Ministerio de Educación y Ciencia, Spain, through a Formación del Profesorado Universitario grant.

C. R. Fernández-Pousa's e-mail address is c.pousa@umh.es.

REFERENCES

1. T. Jansson and J. Jansson, "Temporal self-imaging in single-mode fibers," *J. Opt. Soc. Am.* **71**, 1373–1376 (1981).
2. I. Shake, H. Tahara, S. Kawanishi, and M. Saruwatari, "High-repetition-rate optical pulse generation by using chirped optical pulses," *Electron. Lett.* **34**, 792–793 (1998).
3. S. Arahira, S. Kutsuzawa, Y. Matsui, D. Kanimatsu, and Y. Ogawa, "Repetition-frequency multiplication of mode-locked pulses using fiber dispersion," *J. Lightwave Technol.* **16**, 405–410 (1998).
4. J. Azaña and M. A. Muriel, "Technique for multiplying the repetition rates of periodic trains of pulses by means of a temporal self-imaging effect in chirped fiber gratings," *Opt. Lett.* **24**, 1672–1674 (1999).
5. S. Longhi, M. Marano, P. Laporta, O. Svelto, M. Belmonte, B. Agogliati, L. Arcangeli, V. Pruneri, M. N. Zervas, and M. Ibsen, "40-GHz pulse-train generation at 1.5 μm with a chirped fiber grating as a frequency multiplier," *Opt. Lett.* **25**, 1481–1483 (2000).
6. J. Azaña, P. Kockaert, R. Slavík, L. R. Chen, and S. LaRochelle, "Generation of a 100-GHz optical pulses train by pulse repetition-rate multiplication using superimposed fiber Bragg gratings," *IEEE Photonics Technol. Lett.* **15**, 413–415 (2003).
7. S. Atkins and B. Fischer, "All-optical pulse rate multiplication using fractional Talbot effect and field-to-intensity conversion with cross-gain modulation," *IEEE Photonics Technol. Lett.* **15**, 132–134 (2003).
8. K. Paturski, "The self-imaging phenomenon and its applications," in *Progress in Optics*, E. Wolf, ed. (Elsevier, Amsterdam, 1989), Vol. XXVII, pp. 1–108.
9. A. Kalestynski and B. Smolinska, "Self-restoration of the autoidolon of defective periodic objects," *Opt. Acta* **25**, 125–134 (1978).
10. C. R. Fernández-Pousa, F. Mateos, L. Chantada, M. T. Flores-Arias, C. Bao, M. V. Pérez, and C. Gómez-Reino, "Timing jitter smoothing by Talbot effect. I. Variance," *J. Opt. Soc. Am. B* **21**, 1170–1177 (2004).
11. C. R. Fernández-Pousa, F. Mateos, L. Chantada, M. T. Flores-Arias, C. Bao, M. V. Pérez, and C. Gómez-Reino, "Broadband noise filtering in random sequences of coherent pulses using the temporal Talbot effect," *J. Opt. Soc. Am. B* **21**, 914–922 (2004).
12. D. von der Linde, "Characterization of the noise in continuously operating mode-locked lasers," *Appl. Phys. B: Photo-phys. Laser Chem.* **39**, 201–217 (1986).
13. R. P. Scott, C. Langrock, and B. H. Kolner, "High dynamic range laser amplitude and phase noise measurement techniques," *IEEE J. Sel. Top. Quantum Electron.* **7**, 641–655 (2001).
14. T. Yilmaz, C. M. Depriest, A. Braun, J. H. Abeles, and P. J. Delfyett, "Noise in fundamental and harmonic modelocked semiconductor lasers: experiments and simulations," *IEEE J. Quantum Electron.* **39**, 838–848 (2003).
15. F. Rana, H. L. T. Lee, R. J. Ram, M. E. Grein, L. A. Jiang, E. P. Ippen, and H. A. Haus, "Characterization of the noise and correlations in harmonically mode-locked lasers," *J. Opt. Soc. Am. B* **19**, 2609–2621 (2002).
16. G. P. Agrawal, *Nonlinear Fiber Optics*, 3rd ed. (Academic, Boston, Mass., 2001).
17. M. V. Berry and S. Klein, "Integer, fractional and fractal Talbot effects," *J. Mod. Opt.* **43**, 2139–2164 (1996).
18. N. K. Berger, B. Vodonos, S. Atkins, V. Smulakovsky, A. Bekker, and B. Fischer, "Compression of periodic light pulses using all-optical repetition rate multiplication," *Opt. Commun.* **217**, 343–349 (2003).
19. N. K. Berger, B. Levit, A. Bekker, and B. Fischer, "Compression of periodic optical pulses using temporal fractional Talbot effect," *IEEE Photonics Technol. Lett.* **16**, 1855–1857 (2004).
20. A. Papoulis, *Probability, Random Variables and Stochastic Processes*, 2nd ed. (McGraw-Hill, New York, 1984).
21. J. G. Proakis and D. G. Manolakis, *Digital Signal Processing*, 3rd ed. (Prentice-Hall, Upper Saddle River, N.J., 1996).
22. A. S. Hou, R. S. Tucker, and G. Eisentein, "Pulse compression of an actively modelocked diode laser using linear dispersion in fiber," *IEEE Photonics Technol. Lett.* **2**, 322–324 (1990).
23. T. Yilmaz, C. M. DePriest, P. J. Delfyett, S. Etemad, A. Braun, and J. H. Abeles, "Supermode suppression to below -130 dBc/Hz in a 10 GHz harmonically mode-locked external sigma cavity semiconductor laser," *Opt. Express* **11**, 1090–1095 (2003), <http://www.opticsexpress.org>.
24. J. Azaña and M. A. Muriel, "Temporal self-imaging effects: theory and application for multiplying pulse repetition rates," *IEEE J. Sel. Top. Quantum Electron.* **7**, 728–744 (2001).
25. J. Fatome, S. Pitois, and G. Millot, "Influence of third-order dispersion on the temporal Talbot effect," *Opt. Commun.* **234**, 29–34 (2004).
26. J. Capmany, D. Pastor, S. Sales, and M. A. Muriel, "Pulse distortion in optical fibers and waveguides with arbitrary chromatic dispersion," *J. Opt. Soc. Am. B* **20**, 2523–2533 (2003).
27. J. T. Mok and B. J. Eggleton, "Impact of group delay ripple on repetition-rate multiplication through Talbot self-imaging effect," *Opt. Commun.* **232**, 167–178 (2004).